Analytical approach of Lamb waves coupling in rough isotropic plates

Tony Valier-Brasier,[1,a)] Catherine Potel,[1,b)] Michel Bruneau,[1] and Philippe Gatignol[2]
[1]*Laboratoire d'Acoustique de l'Université du Maine (LAUM) UMR CNRS 6613, Le Mans, France and Fédération Acoustique du Nord-Ouest, (FANO) FR CNRS 3110, France*
[2]*Laboratoire Roberval, UMR UTC-CNRS 6066, Université de Technologie de Compiègne, Compiègne, France*

(Received 25 August 2010; accepted 5 January 2011; published online 16 March 2011)

The present work aims at contributing to the investigation of an analytical method to describe Lamb waves which undergoes Lamb waves coupling when propagating along the rough surfaces of finite extent of isotropic, solid, and infinite plates. The motions considered are assumed to be independent of one of the coordinates for which the component of the displacement is equal to zero (two-dimensional problem). In some respect, the analytical approach is an extension of an analytical model describing the coupling of SH waves due to ridges (on the surface of a plate) parallel to the polarization of the waves, but it is treated in a somewhat different manner because the acoustic field involves here both the longitudinal and the transversal displacements of the Lamb waves. The formalism relies on an integral formulation, using Green's functions which permit to express Lamb waves perturbations, to describe the coupling process between the longitudinal and the transversal components of the forward and the backward propagating Lamb waves, due to the roughness (including the effects of both its depth and its slope). A methodology is given to solve the problem, and results on specific examples (periodic and random rough surfaces) are discussed in order to support the method. © *2011 American Institute of Physics*. [doi:10.1063/1.3552920]

I. INTRODUCTION

The work herein presented aims at providing an analytical model, suitable to highlight the coupling of Lamb waves due to scattering on small one-dimensional irregularities (parallel ridges) of part of the surfaces of homogeneous solid plates. The literature abounds with many papers in which such topics are of principal focus (see Refs. 1–20 and references contained therein), but it is still a challenging topic to obtain tractable and accurate modeling to predict the properties of these fields, having in mind the characterization of the roughness of the boundaries of waveguides. In some respect, the alternative analytical model proposed in the present paper is built upon an analytical model describing SH waves which undergoes scattering (then induces modal coupling) when propagating along the ridged surface of an isotropic solid plate (the ridges being parallel to the polarization of the SH waves considered).[21–24] The waveguide considered is a two-dimensional (x,z) isotropic solid plate in vacuum assumed to be infinite in the y direction, bounded by two parallel surfaces perpendicular to the z axis and having a one-dimensional shape perturbation (small ridges parallel to the y axis of finite extent along the x axis). The two-dimensional Lamb waves considered are assumed to propagate in the plane (x,z) perpendicular to the y axis with longitudinal and transversal polarizations perpendicular to the y axis also (we consider motions independent of the y coordinate for which the y component of the displacement is equal to zero).

As mentioned above, the analytical problem treated here relies fundamentally on the same basic formalism as the one used when only SH waves propagate. But it is treated in a somewhat different manner because the displacement field involves here x and z components of both the longitudinal and the transversal displacements of Lamb waves (these four quantities will henceforth be referred to as the four components of classical plane waves (CCPW) of the displacement field). More particularly, the discussion concerns both (i) the formalism relying on an integral formulation (four coupled integrals) to describe the coupling process (between these four CCPW) due to the roughness of the boundaries of the plate (described by its depth and its slope, and by its length along the x axis), (ii) the expression of the perturbation of each incident (CCPW) at the rough part due to the roughness, using an adapted Green's function in the regularly shaped plate that bounds outwardly the perturbed surfaces of the rough part of the plate considered. With this Green's function, the integral formulation permits to represent the x and z components of the longitudinal and transversal displacement which constitute the Lamb waves perturbations.

Thus, the aim of the paper is twofold: first, to describe the continuously distributed CCPW coupling (along the distributed slight geometrical perturbation of finite extent along the x axis) through the method relying on the Green's theorem and the associated integral formulation mentioned above, second, to discuss results on specific examples to support the method. Note that periodically isotropic plates are considered in order to analyze more deeply the capabilities of the method, especially through the phenomena which occur when considering situations that correspond to the phase-matching between the spatial periodicity of the roughness and the wavelength of the longitudinal and the transversal Lamb waves.

[a)]Electronic mail: tony.valier.brasier@gmail.com.
[b)]Electronic mail: Catherine.Potel@univ-lemans.fr.

II. THE FUNDAMENTAL PROBLEM

A. The corrugated plate

The setup is considered as a two-dimensional domain (x, z), homogeneous solid plate in vacuum, assumed to be infinite in the y direction, bounded by two parallel surfaces perpendicular to the z axis and having 1D shape perturbation (small ridges parallel to the y axis) over a finite length along the x axis (Fig. 1), the solid being characterized by its density ρ and its two Lamé coefficients λ and μ. The ridged surfaces are set respectively at the coordinates z_1 and z_2 (which depend on the coordinate x) and their shape is defined by the local unit vectors $\mathbf{n}_1$ and $\mathbf{n}_2$ normal to the real surfaces of the plate, outwardly directed, given by:

$$\mathbf{n}_q = N_q^{-1}\left[\partial_x h_q\, \mathbf{e}_x + (-1)^q \mathbf{e}_z\right], \quad q = 1, 2, \tag{1a}$$

$\mathbf{e}_x$ and $\mathbf{e}_z$ denoting the unit vectors that have, respectively, the positive direction of the x and z coordinates, with

$$N_q = \sqrt{1 + \left(\partial_x h_q\right)^2}. \tag{1b}$$

They are assumed to be small deviations from the regularly shaped surfaces (set at $\pm L_z/2$) bounding outwardly the perturbed surfaces. The small distance between both surfaces (the regular one and the corrugated one) are denoted $h_1 = (L_z/2) + z_1$ and $h_2 = (L_z/2) - z_2$. An inner plate with regularly shaped surfaces $z = \pm d/2$ is defined as being surrounded by the 1D corrugation.

B. The basic formulation

An harmonic [with a time factor $\exp(i\omega t)$], incoming Lamb wave at the input of the ridged part $x \in (0, \ell)$ of a plate, characterized by its amplitude (depending on both coordinates x and z), is propagating along the plate [domain D, $x \in (0, \infty)$, $z \in (z_1, z_2)$]. The displacement field $\hat{\mathbf{u}}(x, z; t)$ is assumed to be polarized perpendicularly to the y axis [i.e., in the plane (x,z) perpendicularly to the ridges]:

$$\begin{aligned}\hat{\mathbf{u}}(x, z; t) &= \hat{\mathbf{U}}(x, z)\exp(i\omega t)\\ &= \left[\hat{U}_x(x, z)\,\mathbf{e}_x + \hat{U}_z(x, z)\,\mathbf{e}_z\right]\exp(i\omega t).\end{aligned} \tag{2a}$$

Its complex amplitude separates into two parts, namely the longitudinal one $\hat{\mathbf{U}}_L(x, z)$ and the shear one $\hat{\mathbf{U}}_T(x, z)$:

$$\hat{\mathbf{U}}(x, z) = \hat{\mathbf{U}}_L(x, z) + \hat{\mathbf{U}}_T(x, z), \tag{2b}$$

the x and z components of each wave satisfying the following requirements:

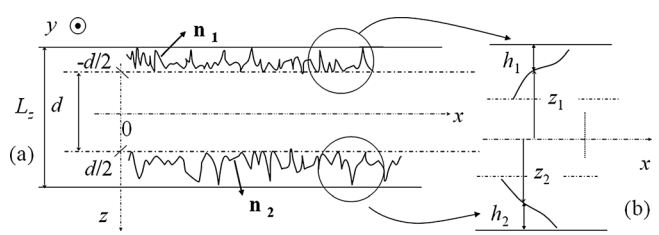

FIG. 1. Sketch of the 2D waveguide with surfaces having small deviations from the regular shape. (a) General view, (b) zoom on the corrugation.

$$\left(\mathbf{curl}\,\hat{\mathbf{U}}_L\right)\cdot\mathbf{e}_y = 0, \text{ i.e., } \partial_z \hat{U}_{L_x}(x, z) = \partial_x \hat{U}_{L_z}(x, z), \tag{3a}$$

$$\operatorname{div}\hat{\mathbf{U}}_T = 0, \text{ i.e., } \partial_z \hat{U}_{T_z}(x, z) = -\partial_x \hat{U}_{T_x}(x, z). \tag{3b}$$

Its behavior is governed by the set of equations, including the propagation equation and the boundary conditions [domain D, $x \in (0, \infty)$, $z \in (z_1, z_2)$], which takes the following form:

$$\begin{cases} \left(\partial_{xx}^2 + \partial_{zz}^2 + k_\eta^2\right)\hat{U}_{\eta_j}(x, z) = -\hat{f}_{\eta_j}(x, z), \ \eta = L, T, \\ \qquad j = x, z, \ \forall (x, z) \in D, \end{cases} \tag{4a}$$

$$\begin{cases} \overline{\overline{\mathbf{T}}}(x, z)\cdot\mathbf{n}_q = \mathbf{0}, \quad \forall x \in (0, \infty), \quad z = z_q(x), \\ \qquad q = 1, 2, \end{cases} \tag{4b}$$

where $k_\eta = \omega/c_\eta$, $c_L = \sqrt{(\lambda + 2\mu)/\rho}$, and $c_T = \sqrt{\mu/\rho}$ being the speeds of, respectively, the longitudinal wave and the shear wave in the homogeneous solid plate, where $\hat{f}_{\eta_j}(x, z)$ represents the source strength, and where $\overline{\overline{\mathbf{T}}}(x, z)$ represents the stress tensor of the total field.

Accounting for expression [Eqs. (1a) and (1b)] of the unit vector $\mathbf{n}_q$, the boundary conditions [Eq. (4b)] on the ridged part of the surfaces z_q $(q = 1, 2)$ of the real waveguide take the following form:

$$\left(\partial_x h_q\right)\hat{T}_{xx}\left(x, z_q\right) + (-1)^q \hat{T}_{xz}\left(x, z_q\right) = 0, \ \forall x, \ q = 1, 2, \tag{5a}$$

$$\left(\partial_x h_q\right)\hat{T}_{xz}\left(x, z_q\right) + (-1)^q \hat{T}_{zz}\left(x, z_q\right) = 0, \ \forall x, \ q = 1, 2. \tag{5b}$$

Hence, invoking the Hooke's law

$$T_{ij} = \lambda\left(\operatorname{div}\hat{\mathbf{U}}\right)\delta_{ij} + \mu\left(\frac{\partial\hat{u}_i}{\partial x_j} + \frac{\partial\hat{u}_j}{\partial x_i}\right), \ i \text{ and } j \text{ being given,} \tag{6a}$$

and accounting for both equations [Eqs. (3a) and (3b)] and the following expression of the normal derivative in the direction of $\mathbf{n}_q$ on the rough boundaries, namely

$$\partial_{n_q} = N_q^{-1}\left[\left(\partial_x h_q\right)\partial_x + (-1)^q \partial_z\right], \quad z = z_q, \quad q = 1, 2, \tag{6b}$$

these boundary conditions imply straightforwardly

$$\begin{aligned}\partial_{n_q}\begin{bmatrix}\hat{U}_{L_x}\\ \hat{U}_{T_x}\end{bmatrix} &= (-1)^{q+1}\left\{\partial_x\left(\hat{U}_{L_z} + \hat{U}_{T_z}\right)\begin{bmatrix}1\\1\end{bmatrix} + \partial_z\begin{bmatrix}\hat{U}_{T_x}\\ \hat{U}_{L_x}\end{bmatrix}\right\}\\ &\quad -\frac{1}{\mu}\left(\partial_x h_q\right)\left\{\lambda\,\partial_z\left(\hat{U}_{L_z} + \hat{U}_{T_z}\right)\begin{bmatrix}1\\1\end{bmatrix}\right.\\ &\quad \left.+(\lambda + \mu)\,\partial_x\left(\hat{U}_{L_x} + \hat{U}_{T_x}\right)\begin{bmatrix}1\\1\end{bmatrix} + \mu\,\partial_x\begin{bmatrix}\hat{U}_{T_x}\\ \hat{U}_{L_x}\end{bmatrix}\right\},\end{aligned} \tag{7a}$$

$$\begin{aligned}\partial_{n_q}\begin{bmatrix}\hat{U}_{L_z}\\ \hat{U}_{T_z}\end{bmatrix} &= (-1)^{q+1}\left\{\frac{\lambda}{\lambda + 2\mu}\partial_x\left(\hat{U}_{L_x} + \hat{U}_{T_x}\right)\begin{bmatrix}1\\1\end{bmatrix}\right.\\ &\quad \left.+\partial_z\begin{bmatrix}\hat{U}_{T_z}\\ \hat{U}_{L_z}\end{bmatrix}\right\} - \frac{\left(\partial_x h_q\right)}{\lambda + 2\mu}\left\{\mu\,\partial_z\left(\hat{U}_{L_x} + \hat{U}_{T_x}\right)\begin{bmatrix}1\\1\end{bmatrix}\right.\\ &\quad +(\lambda + \mu)\,\partial_x\left(\hat{U}_{L_z} + \hat{U}_{T_z}\right)\begin{bmatrix}1\\1\end{bmatrix}\\ &\quad \left.+(\lambda + 2\mu)\,\partial_x\begin{bmatrix}\hat{U}_{T_z}\\ \hat{U}_{L_z}\end{bmatrix}\right\},\end{aligned} \tag{7b}$$

$$\forall x,\ z = z_q,\ q = 1,2.$$

These normal derivatives appear hereafter (Sec. III B) in the integral formulation. They will be expressed in using these last equations [Eqs. (7a) and (7b)].

III. SOLUTIONS FOR THE COUPLED LAMB WAVE PERTURBATIONS

Each component $\hat{U}_{\eta_j}$ $(\eta = L,T\,;\, j = x,z)$ of the displacement field of each CCPW is expressed as the sum of the incoming Lamb wave $\hat{U}^{\text{inc}}_{\eta_j}$ and the scattered wave $\hat{U}^{\text{scatt}}_{\eta_j}$

$$\hat{U}_{\eta_j} = \hat{U}^{\text{inc}}_{\eta_j} + \hat{U}^{\text{scatt}}_{\eta_j}. \tag{8a}$$

The scattered wave is assumed to behave as the superposition of Lamb waves labeled (σ, m)

$$\hat{U}^{\text{scatt}}_{\eta_j} = \sum_{\sigma=1}^{2}\sum_{m=0}^{\infty} \hat{U}^{(\sigma,m)}_{\eta_j}, \tag{8b}$$

where the superscript (σ, m) represents successively Lamb waves as follows:

$(1,0)$ for A0, $(2,0)$ for S0, $(1,1)$ for A1, …, σ denoting the antisymmetrical $(\sigma = 1)$ and symmetrical $(\sigma = 2)$ modes.

A. The integral formulation without roughness

1. Integral formulation

Henceforth, the following notations will be used:

$$\hat{F}^{\text{inc}}_{\eta_j}(x,z) = \int_{-\infty}^{+\infty}\int_{-L_z/2}^{L_z/2} G^{\text{inc}}_{\eta}(x,z;x',z')\hat{f}^{\text{inc}}_{\eta_j}(x',z')\,\mathrm{d}x'\mathrm{d}z', \tag{9a}$$

$$^{(0)}\hat{\Gamma}^{\text{inc}}_{\eta}(x,z)\left\{\hat{U}^{\text{inc}}_{\eta_j}\right\} = \sum_{c=1,2}(-1)^c \int_{-\infty}^{+\infty}\mathrm{d}x' \left[G^{\text{inc}}_{\eta}(x,z;x',z_c) \times \partial_{z_c}\hat{U}^{\text{inc}}_{\eta_j}(x',z_c) - \hat{U}^{\text{inc}}_{\eta_j}(x',z_c)\,\partial_{z_c}G^{\text{inc}}_{\eta}(x,z;x',z_c)\right]_{z_c=(-1)^c L_z/2}. \tag{9b}$$

The four CCPW without roughness (in the external unperturbed waveguide), namely x $(j = 1)$ and z $(j = 2)$ components of both the longitudinal $(\eta = L)$ and the transversal $(\eta = T)$ displacements of the incident Lamb waves $^{(0)}\hat{U}^{\text{inc}}_{\eta_j}(x,z)$ (the only one which exists without roughness), governed by the problem stated above [Eqs. (3a), (3b), (4a), (7a), and (7b)], are solutions of the four coupled integral equations, which involves the domain $D_0 = [x \in (-\infty, \infty),\ z \in (-L_z/2, L_z/2)]$, written as follows,[25,26]

$$^{(0)}\hat{U}^{\text{inc}}_{\eta_j}(x,z) = \hat{F}^{\text{inc}}_{\eta_j}(x,z) + {}^{(0)}\hat{\Gamma}^{\text{inc}}_{\eta}(x,z)\left\{^{(0)}\hat{U}^{\text{inc}}_{\eta_j}\right\}, \tag{10}$$

and are subjected to the boundary conditions [Eqs. (7a) and (7b)].

The first term $\hat{F}^{\text{inc}}_{\eta_j}(x,z)$ in the right hand side of this integral equation is the convolution product of a Green's function (field created by an elementary source) G^{inc}_{η} by a source strength $\hat{f}^{\text{inc}}_{\eta_j}(x,z)$. This first term represents the field created by sources emitting inside the plate. The second term accounts for the field reflected from the boundaries of the plate. This second term involves the same Green's function and the same field as those involved in the first term, and involves also their first derivative with respect to the coordinate normal to the boundaries.

When the Green's function is chosen in such a way that the second term (surface integral) vanishes, the first term represents the field which is solution of the set of Eqs. (4a) and (4b) (Lamb wave) because, in this situation, the Green's function represents the elementary field which satisfies the boundary conditions Eq. (4b) of the Lamb wave considered (situation considered below, Sec. III B).

It is worth noting that the coupling between the four CCPW considered here, expressed through the boundary conditions (7a) and (7b), implies that the function $^{(0)}\hat{\Gamma}^{inc}_{\eta}(x,z)\left\{^{(0)}\hat{U}^{inc}_{\eta_j}\right\}$ depends not only on the CCPW considered $^{(0)}\hat{U}^{inc}_{\eta_j}$ but depends also on the other ones.

2. Components of classical plane wave (CCPW) without roughness

The solutions without roughness are given by the well-known expressions of the Lamb waves, namely for the x and z components of the symmetrical and antisymmetrical Lamb waves, respectively, $(\eta = L,T)$, (Ref. 27) the superscript (inc) being omitted:

$$\begin{cases} ^{(0)}\hat{U}_{\eta_x}(z) = \hat{P}_{\eta_x}\cos\left(k_{\eta_z}z\right)e^{-ik_x x}, \\ ^{(0)}\hat{U}_{\eta_z}(z) = \hat{P}_{\eta_z}\sin\left(k_{\eta_z}z\right)e^{-ik_x x}, \end{cases} \tag{11a}$$

$$\begin{cases} ^{(0)}\hat{U}_{\eta_x}(z) = \hat{Q}_{\eta_x}\sin\left(k_{\eta_z}z\right)e^{-ik_x x}, \\ ^{(0)}\hat{U}_{\eta_z}(z) = \hat{Q}_{\eta_z}\cos\left(k_{\eta_z}z\right)e^{-ik_x x}, \end{cases} \tag{11b}$$

(the amplitudes $\hat{P}_{\eta_x}$ and $\hat{P}_{\eta_z}$, respectively $\hat{Q}_{\eta_x}$ and $\hat{Q}_{\eta_z}$, being not independent one from the others), the wavenumbers k_x and k_{η_z} being solutions of the following Rayleigh-Lamb equations, for the symmetrical and antisymmetrical modes respectively,

$$\frac{\tan\left(k_{T_z}L_z/2\right)}{\tan\left(k_{L_z}L_z/2\right)} = -\frac{4k_x^2 k_{L_z}k_{T_z}}{\left(k_{T_z}^2 - k_x^2\right)^2}, \tag{11c}$$

$$\frac{\tan\left(k_{T_z}L_z/2\right)}{\tan\left(k_{L_z}L_z/2\right)} = -\frac{\left(k_{T_z}^2 - k_x^2\right)^2}{4k_x^2 k_{L_z}k_{T_z}}, \tag{11d}$$

where (dispersion equation)

$$k_x^2 + k_{\eta_z}^2 = k_\eta^2, \qquad \eta = L,\ T. \tag{11e}$$

In the formalism used herein, the solution without roughness depends on the sources that are set on the surfaces of the plate which are located along the x axis upstream from the roughness so that an incoming Lamb wave traveling in the x direction is generated at the input of the rough part of the domain *(D)* of interest. The source strength $\hat{f}_{\eta_j}(x,z)$ [Eq. (4a)] is then achieved by assuming a continuous distribution of fluctuating (namely harmonic) displacements on the surfaces $z = \pm L_z/2$ of the plate which is a given function of the position x. Herein, this continuous distribution must be written as the superposition of four functions of the abscissa x, each

one being assumed to generate one of the four given CCPW (x- and z-components of longitudinal and transversal displacements). Actually, the capacity of real sources for generating such displacement fields depends critically upon the spatial distribution of amplitude and phase of surface displacement over their surfaces (the source control procedure is beyond the scope of this paper).

The Green's functions, which enable differential equations and boundary conditions to be combined into integral equations, are introduced here in such a way that the four source functions $\hat{F}^{\mathrm{inc}}_{\eta_j}(x,\,z)$ which appear in the right-hand side of Eq. (10) represent the amplitude of each mode ${}^{(0)}\hat{U}^{\mathrm{inc}}_{\eta_j}$ of the incoming Lamb wave in the whole domain (D_0) without roughness. Therefore, the Green's functions must be chosen in such a way that the surface integral in Eq. (10) vanishes:

$$ {}^{(0)}\hat{\Gamma}^{\mathrm{inc}}_{\eta}(x,\,z)\left\{{}^{(0)}\hat{U}^{\mathrm{inc}}_{\eta_j}\right\}=0. \tag{12}$$

as mentioned above [below Eq. (10)].

3. The Green's functions

For a given Lamb wave [denoted (σ,m) in Eq. (8b) and in the following Sec. III B] the Green's functions chosen are governed by the set of equations, including the propagation equation and the boundary conditions [in the domain D_0, $x\in(-\infty,\,\infty),\ z\in(-L_z/2,\,L_z/2)$]:

$$\begin{cases}\left(\partial^2_{xx}+\partial^2_{zz}+k^2_{\eta}\right)G_{\eta}(x,z;x_0,z_0)=-\delta(x-x_0)\,\delta(z-z_0), \\ \qquad \forall(x,\,z)\in D_0, & \text{(13a)}\\ \left(\partial_z-\mathrm{i}k_{\eta}\,Y_{\eta}\right)G_{\eta}=0, \quad \forall x,\ z=-L_z/2, & \text{(13b)}\\ \left(\partial_z+\mathrm{i}k_{\eta}\,Y_{\eta}\right)G_{\eta}=0, \quad \forall x,\ z=+L_z/2, & \text{(13c)}\end{cases}$$

with

$$Y_{\eta}=-\mathrm{i}\frac{k_{\eta_z}}{k_{\eta}}\tan\left(k_{\eta_z}L_z/2\right), \tag{13d}$$

δ being the Dirac function, and k_{η_z} being given in Eq. (11e).

It can be readily verified that Eq. (12) is satisfied with these Green's functions because they satisfy such boundary conditions.

This Green's functions $G_{\eta}(x,z;x',z')$, solutions of Eqs. (13a)–(13c), is represented herein by a Fourier integral (in χ), both for the longitudinal ($\eta=L$) and transversal ($\eta=T$) waves:

$$G_{\eta}(x,z;x_0,z_0)=\int_{-\infty}^{+\infty}h_{\eta}(x,z;\chi,z_0)\ \exp(i\,\chi\,x_0)\,\mathrm{d}\chi. \tag{14}$$

Invoking the dispersion relationship

$$\chi^2+\kappa^2_{\eta_z}=k^2_{\eta}, \tag{15}$$

and inserting expression (14) into Eq. (13a) gives

$$\begin{aligned}&\int_{-\infty}^{+\infty}\left[\partial^2_{zz}+\kappa^2_{\eta_z}\right]h_{\eta}(x,z;\chi,z_0)\exp(i\,\chi\,x_0)\,\mathrm{d}\chi\\ &\qquad=-\delta(x-x_0)\,\delta(z-z_0).\end{aligned} \tag{16a}$$

Hence, multiplying this equation by $\exp(-i\,\chi\,x_0)$, integrating over the coordinate x, and applying the result

$$\frac{1}{2\,\pi}\int_{-\infty}^{+\infty}\exp[\mathrm{i}(\chi-\chi')\,x_0]\,\mathrm{d}\,x_0=\delta(\chi-\chi'), \tag{16b}$$

leads to

$$\left[\partial^2_{zz}+\kappa^2_{\eta_z}\right]\,h_{\eta}(x,z;\chi,z_0)=-\frac{1}{2\,\pi}\exp(-i\,\chi\,x)\,\delta\,(z-z_0). \tag{17}$$

The solution h_{η}, subjected to the boundary conditions (13b) and (13c), can be expressed as follows:[25,26]

$$h_{\eta}(x,z;\chi,z_0)=-\frac{\exp(-i\,\chi\,x)}{2\,\pi}\,\frac{\cos\left[\kappa_{\eta_z}z_<+\left(\kappa_{\eta_z}-k_{\eta_z}\right)(L_z/2)+\beta\right]\cos\left[\kappa_{\eta_z}z_>-\left(\kappa_{\eta_z}-k_{\eta_z}\right)(L_z/2)-\beta\right]}{\kappa_{\eta_z}\sin\left[\left(\kappa_{\eta_z}-k_{\eta_z}\right)L_z+2\,\beta\right]}, \tag{18a}$$

where

$$z_>=z \text{ and } z_<=z_0 \text{ if } z>z_0, \tag{18b}$$

$$z_>=z_0 \text{ and } z_<=z \text{ if } z<z_0, \tag{18c}$$

with $\beta=0$ and $\pi/2$ for even (cosine) and odd (sine) Lamb waves, respectively.

The integral (16)–(18) can be handled numerically straightforwardly (see Sec. III B 2 below)

When using this Green's function (see next Sec. III B), for the roughness given by the coordinate $z_0=z_1<0$, near the wall set at $(-L_z/2)$,

$$z_>=z \text{ et } z_<=z_1, \tag{19a}$$

and for the roughness given by the coordinate $z_0=z_2>0$, near the wall set at $(+L_z/2)$

$$z_>=z_2 \text{ et } z_<=z. \tag{19b}$$

B. The integral formulation with roughness and the iterative solution

1. The integral formulation

In addition to the notations (9a) and (9b) given above, the following notations will be used:

$$\begin{aligned}\hat{\Gamma}^{(\sigma,m)}_{\eta}(x,z)\left\{\hat{U}_{\eta_j}\right\}=\sum_{q=1,2}\int_{-\infty}^{+\infty}\mathrm{d}x'\Big[&G^{(\sigma,m)}_{\eta}\left(x,z;x',z'_q\right)\\ &\times\partial_{n_q}\hat{U}_{\eta_j}\left(x',z'_q\right)-\hat{U}_{\eta_j}\left(x',z'_q\right)\partial_{n_q}G^{(\sigma,m)}_{\eta}\left(x,z;x',z'_q\right)\Big]_{z'_q=z'_q(x')},\end{aligned} \tag{20a}$$

$$\delta\hat{\Gamma}^{(\sigma,m)}_{\eta}(x,\,z)=\left[\hat{\Gamma}^{(\sigma,m)}_{\eta}(x,\,z)-{}^{(0)}\hat{\Gamma}^{(\sigma,m)}_{\eta}(x,\,z)\right]. \tag{20b}$$

The four quasi-CCPW with roughness $\hat{U}_{\eta_j}^{(\sigma,m)}(x,z)$, namely x- ($j=1$) and z- ($j=2$) components of both the longitudinal ($\eta=L$) and the transversal ($\eta=T$) displacements of the Lamb waves, governed by the problem stated above [Eqs. (3a), (3b), (4a), (7a), and (7b)], are solutions of the four coupled integral equations, written as follows,[25,26] which involves the domain $D=[x\in(-\infty,\infty), z\in(z_1, z_2)]$:

$$\hat{U}_{\eta_j}^{(\sigma,m)}(x,z)=\hat{F}_{\eta_j}^{(\sigma,m)}(x,z)+\hat{\Gamma}_{\eta}^{(\sigma,m)}(x,z)\left\{\hat{U}_{\eta_j}\right\} \tag{21}$$

and are subjected to the boundary conditions (7a) and (7a).

Owing to the roughness, the second term in the right-hand side of the integral equation does not vanish. Therefore, it represents the effect of the roughness on Lamb waves created by sources set upward the roughness part of the plate [function $\hat{F}_{\eta_j}^{(\sigma,m)}(x,z)$], which are incident at the input of the rough part.

As already mentioned, it is worthwhile commenting that the coupling between the four CCPW considered here, expressed through the boundary conditions (7a) and (7b), implies that the function $\hat{\Gamma}_{\eta}^{(\sigma,m)}(x,z)\{\hat{U}_{\eta_j}\}$ depends not only on the CCPW considered $\hat{U}_{\eta_j}$ but depends also on the other ones [through Eqs. (7a) and (7b)].

2. Iterative solution

Using an iterative method to express the amplitude of each mode $\hat{U}_{\eta_j}^{(\sigma,m)}(x,z)$ in the domain $(D\subset D_0)$, which assumes that the coupling functions contained in the right-hand side of Eq. (21) are small quantities compared to the source term $\hat{F}_{\eta_j}^{(\sigma,m)}$, thus the Nth-order solution of Eq. (21) for each mode $\hat{U}_{\eta_j}^{(\sigma,m)}(x,z)$ is written as follows:

$$\begin{aligned}{}^{[N]}\hat{U}_{\eta_j}^{(\sigma,m)}(x,z)={}&{}^{(0)}\hat{U}_{\eta_j}^{(\sigma,m)}(x,z)+{}^{(1)}\hat{U}_{\eta_j}^{(\sigma,m)}(x,z)\\&+\cdots+{}^{(N)}\hat{U}_{\eta_j}^{(\sigma,m)}(x,z),\end{aligned} \tag{22}$$

where ${}^{[N]}\hat{U}_{\eta_j}^{(\sigma,m)}(x,z)$ denotes the Nth-order perturbation expansion for $\hat{U}_{\eta_j}^{(\sigma,m)}(x,z)$,

$${}^{[0]}\hat{U}_{\eta_j}^{(\sigma,m)}(x,z)={}^{(0)}\hat{U}_{\eta_j}^{(\sigma,m)}(x,z)=\hat{U}_{\eta_j}^{inc}(x,z)=\hat{F}_{\eta_j}^{inc}(x,z), \tag{23}$$

[Eqs. (10) and (12)] being the zero-order approximation (the solution without roughness), ${}^{(1)}\hat{U}_{\eta_j}^{(\sigma,m)}(x,z)$ the first order correction term, and so on.

The solution without roughness being given by Eqs. (10) and (12), the first-order solutions of Eq. (21) (Born approximation, discarding the second-order term) are straightforwardly given by writing

$$\begin{aligned}{}^{(0)}\hat{U}_{\eta_j}^{(\sigma,m)}(x,z)+{}^{(1)}\hat{U}_{\eta_j}^{(\sigma,m)}(x,z)\cong{}&\hat{S}_{\eta_j}^{(\sigma,m)}(x,z)\\&+\hat{\Gamma}_{\eta}^{(\sigma,m)}(x,z)\left\{\hat{U}_{\eta_j}^{\text{inc}}\right\},\end{aligned} \tag{24}$$

where $\hat{S}_{\eta_j}^{(\sigma,m)}(x,z)=\hat{F}_{\eta_j}^{\text{inc}}(x,z)$ or 0, depending on whether (σ,m) represents the incident wave or not, and where ${}^{(0)}\hat{U}_{\eta_j}^{(\sigma,m)}$ is given by Eq. (23).

It follows that the first order perturbation term has the form, for any superscripts (σ,m),

$${}^{(1)}\hat{U}_{\eta_j}^{(\sigma,m)}(x,z)\cong\delta\hat{\Gamma}_{\eta}^{(\sigma,m)}(x,z)\left\{{}^{(0)}\hat{U}_{\eta_j}^{\text{inc}}\right\}. \tag{25}$$

In this last expression, the scattered Lamb wave (σ,m), which does not exist at the zero-order approximation (${}^{(0)}\hat{U}_{\eta_j}^{(\sigma,m)}=0$ without roughness), appears to be created by a "secondary" source which represents the effect on this Lamb wave (σ,m) of the scattering of the incident wave ${}^{(0)}\hat{U}_{\eta_j}^{\text{inc}}$ on the rough surface. This secondary source behaves as a surface source (on the boundary of the plate) whose strength, at each location of the roughness, is proportional to both: (i) the amplitude and its first normal derivative (in the direction $\mathbf{n}_q$ on the rough boundary) of the incident Lamb wave (which provides energy to the system), (ii) and the operator $\delta\hat{\Gamma}_{\eta}^{(\sigma,m)}$ acting on them, which departs from the operator $\delta\hat{\Gamma}_{\eta}^{\text{inc}}=\hat{\Gamma}_{\eta}^{\text{inc}}-{}^{(0)}\hat{\Gamma}_{\eta}^{\text{inc}}$ because it is associated to the scattered wave considered (σ,m).

Finally, the [Nth]-order correction terms of the iterative solutions of Eq. (21) are given by

$${}^{(N)}\hat{U}_{\eta_j}^{(\sigma,m)}(x,z)\cong\sum_{\alpha=1}^{2}\sum_{r=0}^{\infty}\delta\hat{\Gamma}_{\eta}^{(\sigma,m)}\left\{{}^{(N-1)}\hat{U}_{\eta_j}^{(\alpha,r)}\right\}, \tag{26}$$

where superscripts (α,r) denote the Lamb waves considered.

It is worthwhile commenting that the right hand side integral represents the boundary modal coupling due to the shape profile of the roughness.

3. Numerical computation

Despite the quite complicated form of these four coupled integral equations, it is a straightforward, if tedious, procedure to numerically solve them. First the Green's function must be calculated. In evaluating this Green's function numerically, there are two possible approaches.

In a first approach, the integrals are numerically integrated directly along the contour C $\{Q_1(\to-\infty); P_1(=-k_\eta-i\varepsilon); O; P_2(=+k_\eta+i\varepsilon); Q_2(\to+\infty)\}$ shown in Fig. 2, where ε is a small quantity.[28] This contour is deformed onto the real axis, in order to avoid the poles of the integrand, above (below) any poles on the negative (positive) real axis. In the results presented in Fig. 2, the contour C is limited to a finite interval $[Q_1, Q_2]$ (the integrals converge always very rapidly).

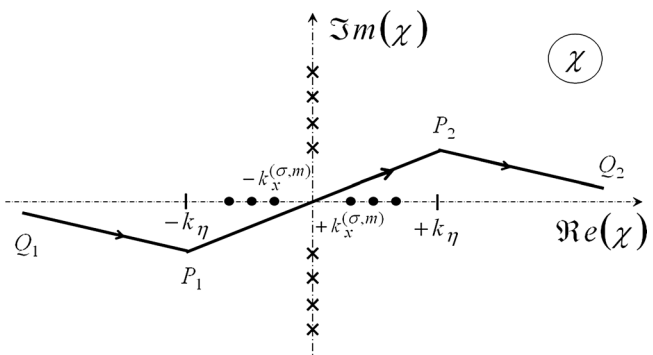

FIG. 2. Complex integration path in the complex plane of χ.

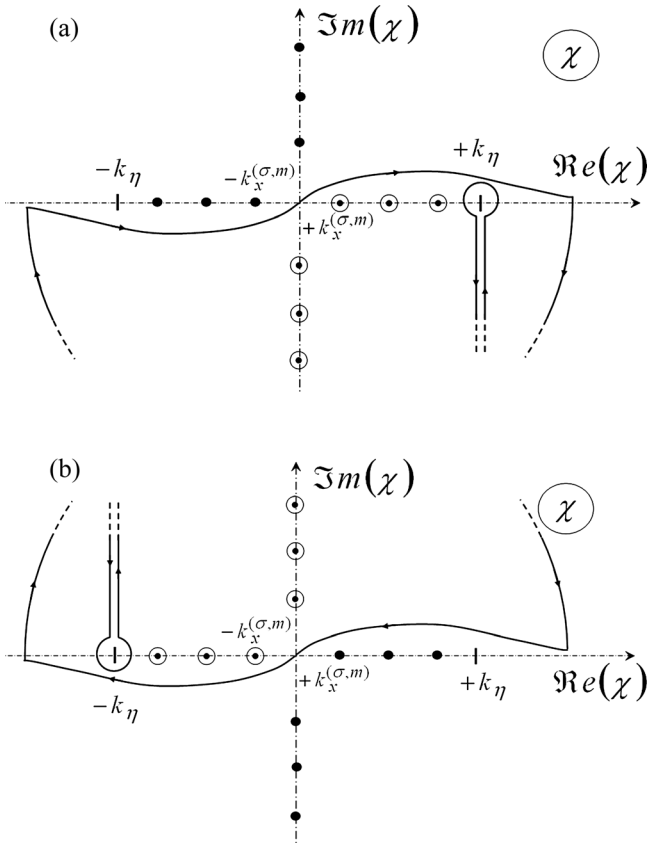

FIG. 3. Complex integration paths in the complex plane of χ. (a) $x > x_0$, the integration path (a) is closed by a semicircle of infinite radius in the lower half-plane, (b) $x < x_0$, the integration path (b) is closed by a semicircle of infinite radius in the upper half-plane.

In a second approach, the contour C is closed by a semicircle of infinite radius in the upper (lower) half-plane χ depending on respectively $x < x_0$ ($x > x_0$) with the singularity of the integrand at $\chi = -k_\eta$ ($\chi = +k_\eta$) excluded from the area enclosed (branch cuts, Fig. 3).

Using Cauchy's theorem, the integrals can be expressed as the sum of residue terms plus an integral along the branch cuts.

The poles are defined by [see Eq. (18a)]

$$\sin\left[\left(\kappa_{\eta_z} - k_{z_\eta}\right)L_z + 2\beta\right] = 0, \tag{27}$$

[κ_{η_z} depending on χ through Eq. (15)], which occurs when

$$\chi = \pm\sqrt{\left(k_x^{(\sigma,m)}\right)^2 - \frac{2p\pi}{L_z}k_{\eta_z}^{(\sigma,m)} - \left(\frac{2p\pi}{L_z}\right)^2}, \text{ if } \beta = 0, \tag{28a}$$

and when

$$\chi = \pm\sqrt{\left(k_x^{(\sigma,m)}\right)^2 - \frac{2(p-1)\pi}{L_z}k_{\eta_z}^{(\sigma,m)} - \left(\frac{2(p-1)\pi}{L_z}\right)^2}, \quad \text{if } \beta = \pi/2, \tag{28b}$$

p being an integer.

It is worthwhile to point out that the residue contributions can be interpreted as a superposition of symmetrical ($\beta = 0$) and antisymmetrical ($\beta = \pi/2$) Lamb waves and that the first two residues are predominant, the other ones do not contribute significantly (this is related to the rapid convergence in the first approach mentioned above). In this present approach, the integrals along the branch cuts must be calculated numerically, leading to calculus which takes more time than those in the first approach.

IV. RESULTS AND DISCUSSION

Being concerned by the efficiency of the method, we give several applications here: those where (i) the roughness, which can be considered as very thin regarding the characteristic dimension of the acoustic domain, is a one dimensional periodically corrugated surface; (ii) relationships (dispersion law and phase matching law) between the spatial period of the corrugation and the x-components of the wavenumbers considered (incident and scattered Lamb waves) are, in the frequency range chosen, such as both a stop-band for the incident Lamb wave (primary wave) and a phase matching for the contra-propagative purely scattered Lamb wave considered (counter-propagative secondary wave); (iii) a quasi-random roughness, yet typical of engineering problems, induces a decreasing of the amplitude of a Lamb wave when propagating along the rough surface. For an incident Lamb wave A0 and a scattered Lamb wave S0, the phase-matching relationships are represented in Fig. 4 for the results given in Figs. 5 and 6, and, for an incident Lamb wave S0 and a scattered Lamb wave A1, they are represented in Fig. 7 for the results given in Fig. 8. The material constituting the solid plate is aluminum, characterized by its density $\rho = 2700$ kg.m^{-3}, and the speeds of longitudinal and transversal waves $c_L = 6430$ m.s^{-1} and $c_T = 3140$ m.s^{-1}, respectively.

In Fig. 4 (resp. Fig. 7), the solid lines represent the dispersion curves for S0 and A0 (resp. S0 and A1) Lamb waves given by the Rayleigh–Lamb Eq. (27) and the dashed lines represent the phase-matching (phonon relationship) for A0 (resp. S0) Lamb waves given by

$$k_x^{inc} + k_x^{(\sigma,m)} - \frac{2\pi}{\Lambda} = 0. \tag{29}$$

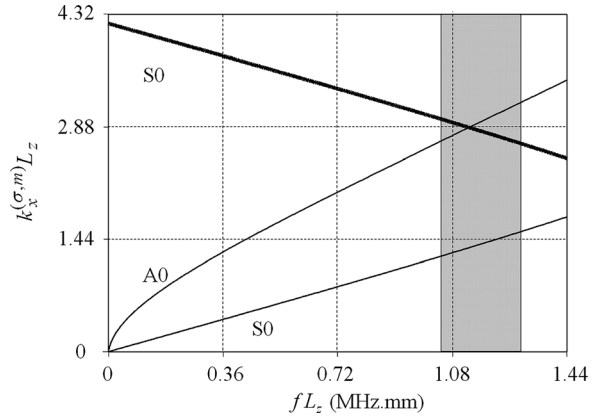

FIG. 4. Dispersion curves (thin solid lines) and coupling curve (thick solid line) of Lamb waves, in the plane (frequency × thickness $f \times L_z$; wave number×thickness $k_x^{(\sigma,m)} \times L_z$).

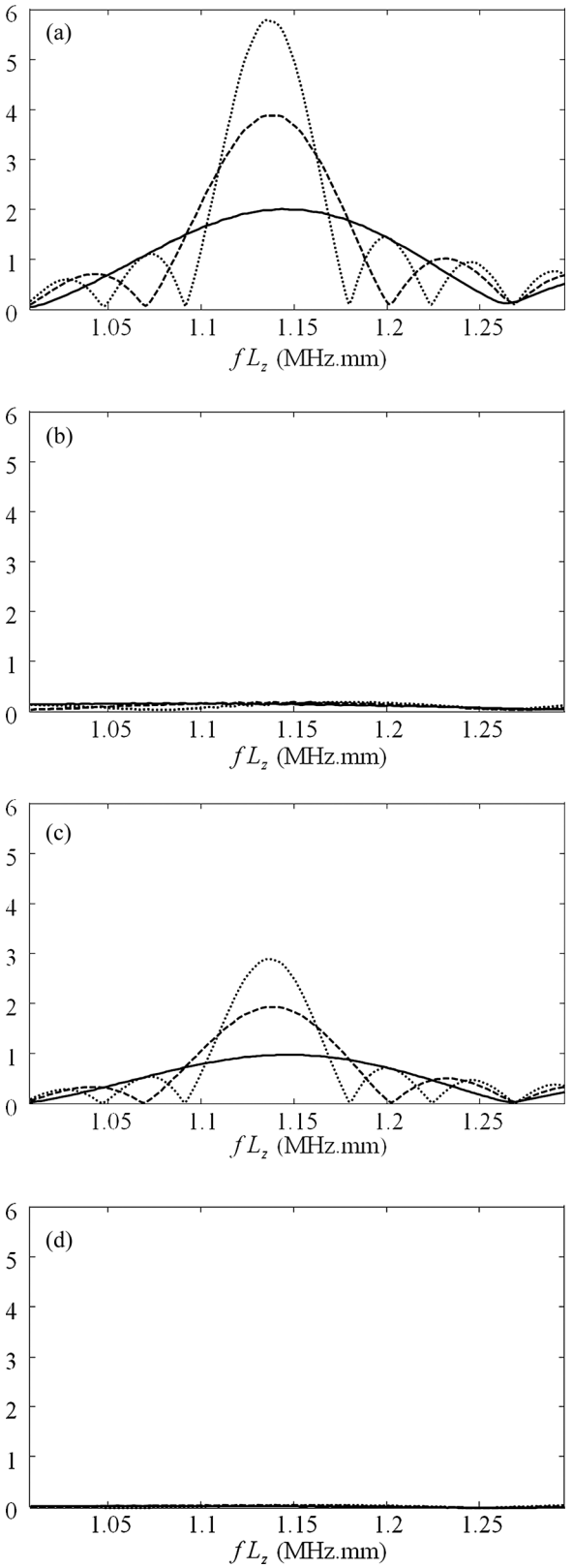

FIG. 5. Modulus of the normalized x-component $\hat{U}_{x_N}^{(\sigma=1,m=0)}$ of the displacement field of the scattered Lamb wave A0 at the points (a) $(x=0, z=L_z/4)$ and (b) $(x=\ell, z=L_z/4)$, as a function of the product frequency×thickness $(f \times L_z)$. Modulus of the normalized z component $\hat{U}_{z_N}^{(\sigma=1,m=0)}$ of the displacement field of the scattered Lamb wave A0 at the points (c) $(x=0, z=L_z/4)$ and (d) $(x=\ell, z=L_z/4)$, as a function of the product frequency×thickness $(f \times L_z)$. Full solid line: $\ell = 10\,\Lambda$; dashed line: $\ell = 20\,\Lambda$; dotted line: $\ell = 30\,\Lambda$ where ℓ is the length of corrugation. Sawtooth profile (see Fig. 9).

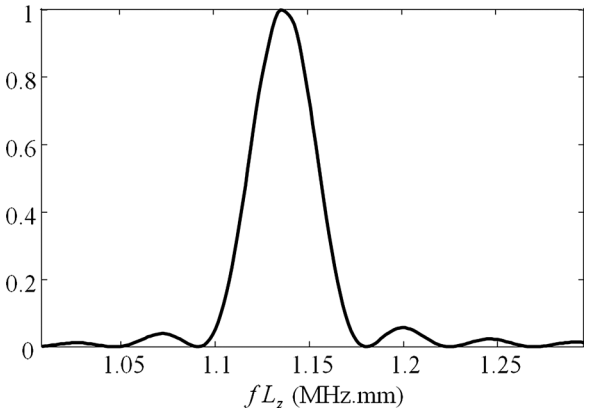

FIG. 6. Normalized square of the z-component $\hat{U}_z^{(\sigma=1,m=0)}$ of the displacement field of the scattered Lamb wave A0 at the point $(x=0, z=L_z/2)$ as a function of the product frequency×thickness $(f \times L_z)$. Sawtooth profile (see Fig. 9).

The roughness considered in Figs. 5 and 6 is a periodically sawtooth profile (isosceles triangles shown in Fig. 9) of finite extent ℓ, of depth h, and of spatial period Λ, set at one of the boundaries of the plate as presented in Sec. II A. The frequency range of interest, given by the product $fL_z \in (1.0, 1.3)$ MHz mm, is represented with gray in Fig. 4. It is chosen in such a way that the phase matching given by Eq. (29) occurs. The roughness considered in Fig. 8 is a sinusoidal profile set at one of the boundaries of the plate as shown in Fig. 10 (the notations are the same as those used for the sawtooth profile).

For three values of the number of teeth ℓ/Λ (10, 20, and 30), Figs. 5(a) and 5(b) show, respectively, at the input $(x=0)$ and at the output $(x=\ell)$ of the corrugated domain $(z=L_z/4)$, the x-component of the normalized displacement of the back-scattered Lamb wave A0 (created by its strong coupling with the incoming Lamb wave S0 through the sawtooth corrugated surface) as a function of the frequency, in the frequency range where the phase-matching mentioned above occurs (the normalizing factor being the amplitude of the x-component of the incident wave). At $x=0$, the shape of the curve [Fig. 5(a)] is the one expected, i.e.,

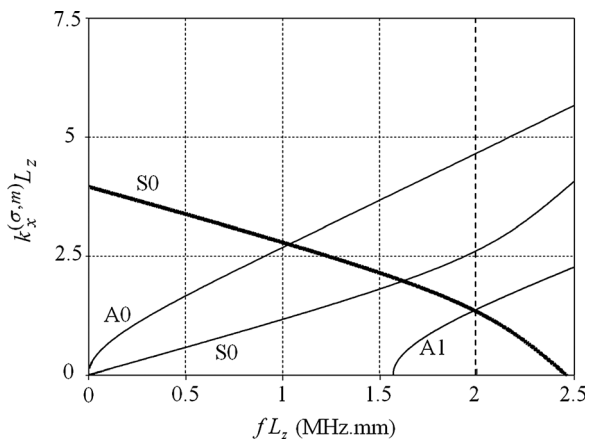

FIG. 7. Dispersion curves (thin solid lines) and coupling curve (thick solid line) of Lamb waves, in the plane (frequency × thickness $f \times L_z$; wave number×thickness $k_x^{(\sigma,m)} \times L_z$).

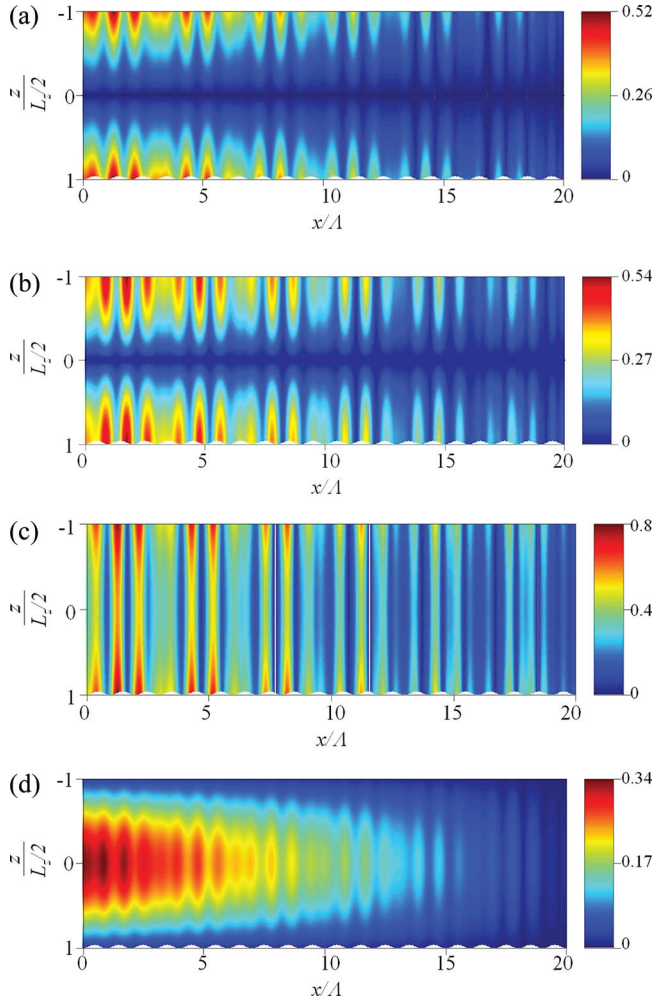

FIG. 8. (Color online) Modulus of the displacement fields which constitute the scattered Lamb wave A1 as a function of the adimensionalized locations x/Λ (abscissa) and $2z/L_z$ (ordinate). (a) x-component $\hat{U}_{L_x}^{(\sigma=1,m=1)}$ of the longitudinal wave, (b) x-component $\hat{U}_{T_x}^{(\sigma=1,m=1)}$ of the transversal wave, (c) z-component $\hat{U}_{L_z}^{(\sigma=1,m=1)}$ of the longitudinal wave and (d) z-component $\hat{U}_{T_z}^{(\sigma=1,m=1)}$ of the transversal wave. Sinusoidal profile (see Fig. 10).

approximately a cardinal sine (sinc).[29] At $x = \ell$ [Fig. 5(b)], it vanishes because this backward wave is not created at the output of the corrugation domain. The situations presented on Figs. 5(c) and 5(d) are the same as the preceding ones Figs. 5(a) and 5(b) except that the component of the Lamb

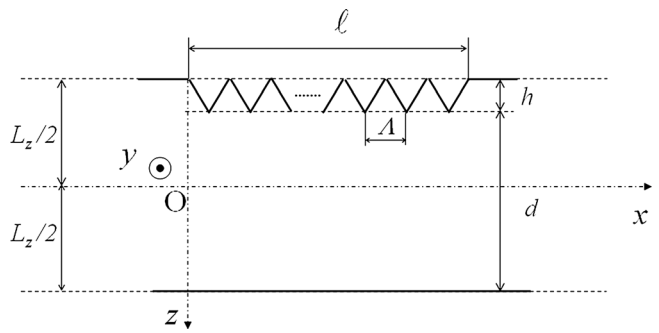

FIG. 9. Regularly distributed sawtooth profile on one side of the plate used for Figs. 5 and 6. Spatial period Λ, height of the teeth h, length of roughness ℓ, thickness of the outer waveguide L_z, thickness of the inner waveguide d such that $L_z/\Lambda = 0.686$, $h/d = 0.043$.

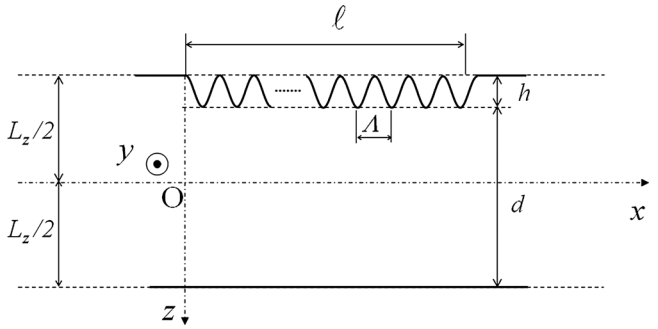

FIG. 10. Sinusoidal profile on one side of the plate used for Fig. 8. Spatial period Λ, height of the teeth h, length of roughness ℓ, thickness of the outer waveguide L_z, thickness of the inner waveguide d such that $L_z/\Lambda = 0.625$, $h/d = 0.02$, $\ell/\Lambda = 20$.

wave A0 considered is the z-component. The results show that the amplitude, which is normalized by the same factor as the one used in the x-component, is lower. This is due to the fact that the z-component of the longitudinal wave vanishes (it is evanescent in this frequency range).

Figure 6 presents the theoretical result obtained here for the square of the z component of the displacement field expressed at the input of the roughness $x = 0$, on the upper surface of the plate $z = L_z/2$, normalized to unity, as a function of the frequency, in the frequency range mentioned above. Especially concerning the shape of the curves, this result shows a good agreement with those available in the literature.[29]

A backscattered Lamb wave A1, created by its strong coupling with the incoming Lamb wave S0 through the sinusoidal corrugated surface, is presented in Fig. 8 as a function of the normalized coordinates, namely the coordinate x/Λ and $z/(L_z/2)$. The scales give the relative amplitude of each CCPW ($\hat{U}_{L_x}$, $\hat{U}_{L_z}$, $\hat{U}_{T_x}$, and $\hat{U}_{T_z}$). The periodic oscillations which appear from the right part to the left part of the diagrams are directly linked to the phase-matching relationship which occurs at the frequency given by $fL_z = 1.975$ MHz.mm (Fig. 7). As predicted, the wave is created from the right to the left. The x-components are antisymmetrical and the z components are symmetrical with respect to $z = 0$, as expected.

Finally, it is of interest to investigate the modeling presented in this paper when applying it to a class of problem which is typical of engineering situations, as sanded or shot blasted plates for example. In this frame, the behavior of the amplitude of an incoming Lamb wave A0 is investigated when the roughness is assumed to have a pseudorandom profile which exhibits several spatial periods (usually, in practice, rough surfaces exhibit a limited number of dominant spatial periodicities), one of them verifying a phase matching with the Lamb wave considered for the frequency chosen.

The power spectral density (PSD), namely the Fourier transform with respect to the abscissa x of the autocovariance function of the depth of the roughness, as a function of the inverse adimensional spatial wavelength, is depicted in Fig. 11. Being given the value of the product of the wavenumber k_x of the Lamb wave A0 along the x axis by the

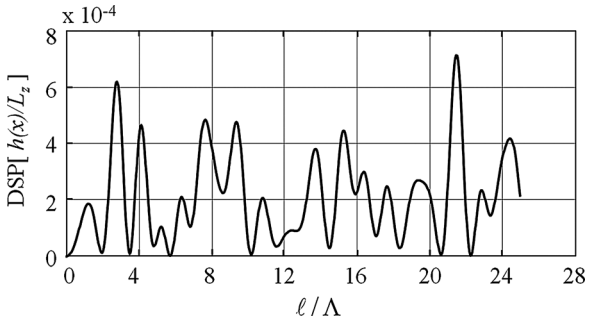

FIG. 11. Power spectral density (PSD) of the pseudorandom roughness as a function of the inverse adimensional spatial period.

length ℓ of the roughness $(k_x\ell = 25.6)$, the phase-matching relationship $k_x = \pi/\Lambda$ leads to an inverse adimensional spatial period $\ell/\Lambda \cong 8$ which is very close to one of the maxima of the PSD.

This result leads to eight oscillations in the amplitude of the Lamb wave A0 as a function of the adimensional distance $k_x x$ along the rough part of the plate as shown in Figs. 12(a) and 12(b) [the first four appear clearly over the interval $(0,\ \ell/2)$].

Figures 12(a) and 12(b) show, respectively, the amplitude (arbitrary unit) of the components $\hat{U}_{L_z}$ and $\hat{U}_{T_z}$ of the displacement field in the middle $(z = 0)$of the plate along its rough part [the components $\hat{U}_{L_x}$ and $\hat{U}_{T_x}$ vanish at the coordinate $(z = 0)$]. The mean decreasing can be interpreted as an exponential decreasing $\exp(-\kappa_x x)$, leading to an adimensional attenuation factor $\kappa_x L_z$ of the order of magnitude of 0.01–0.03. This result is consistent with those obtained experimentally with a shot blasted isotropic plate having approximately the same average adimensional depth of roughness.[30]

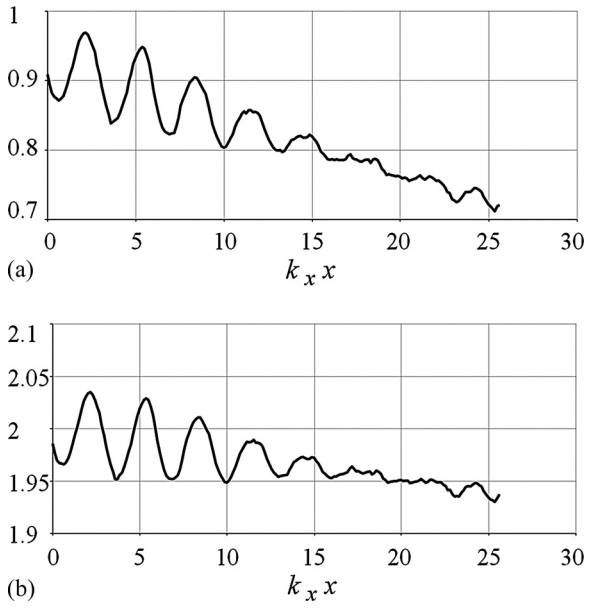

FIG. 12. Amplitude (modulus, arbitrary unit) of the components $\hat{U}_{L_z}$ (a) and $\hat{U}_{T_z}$ (b) of the displacement field along the rough part of the plate, as functions of the product of the wavenumber along the plate with the abscissa x.

V. SUMMARY AND CONCLUSION

This contribution to the investigation of a new method to solve problems of scattering of Lamb waves on rough surfaces of finite extent, in homogeneous solid plates of infinite extent, involves four coupled scalar integral equations and adapted Green's functions for each component of each classical plane wave. The theoretical results can be handled straightforwardly numerically when the corrugations are assumed to be small deviations from the regularly shaped surface of the plate. Especially, the Fourier integrals which express the Green's functions converge very rapidly, emphasizing the role played by the first two poles, thus leading to both the symmetrical and antisymmetrical Lamb waves considered. These theoretical results show that both the depth and the slope of the roughness play important roles in the scattering process, i.e., when the incident field propagating along the corrugated part of the waveguide undergoes scattering, initiating the coupling of Lamb waves.

The examples presented have highlighted the advantage of the method in having given expected results when retrodiffusion (backward scattering) occurs, that is when a stopband plays a very important role for the Lamb waves considered, and when a Lamb wave A0 propagates along a quasirandom roughness. Given the specificity of these examples, there is seen to be quite close agreement between theoretical and expected results, thereby supporting the method presented in this paper. Therefore, it seems that this method provides a viable approach to solve the class of problems considered, having in mind means of predicting the effects of roughness in engineering problems. Actually, it remains to be seen whether the proposed methodology is efficient when applied to problems of real engineering significance.

ACKNOWLEDGMENTS

Support from CNRS through the research group GDR-2501 and from "Fédération d'Acoustique du Nord Ouest" (FANO, FR CNRS 3110) are gratefully acknowledged. The authors want to thank their colleagues from "Laboratoire Ondes et Milieux Complexes" (LOMC, FRE CNRS 3110) in Le Havre for their helpful discussions. They also want to thank the reviewer for helpful suggestions.

[1]O. I. Lobkis and D. E. Chimenti, J. Acoust. Soc. Am. **102**, 143 (1997).
[2]D. E. Chimenti and O. I. Lobkis, Ultrasonics **36**, 155 (1998).
[3]A. Demma, P. Cawley, and M. Lowe, J. Acoust. Soc. Am. **113**, 1880 (2003).
[4]V. Pagneux and A. Maurel, Proc. R. Soc. Ser. A: Math. Physic. Eng. Sci. **458**, 1913 (2002).
[5]T. W. Dawson and J. A. Fawcett, J. Acoust. Soc. Am. **87**, 1110 (1990).
[6]M. A. Hawwa, J. Acoust. Soc. Am. **102**, 137 (1997).
[7]V. Pagneux and A. Maurel, Proc. R. Soc. Ser. A: Math. Physic. Eng. Sci. **462**, 1315 (2006).
[8]S. Banerjee and T. Kundu, J. Acoust. Soc. Am. **119**, 2006 (2006).
[9]S. Banerjee and T. Kundu, Int. J. Solids Struct. **43**, 6551 (2006).
[10]G. Shkerdin and C. Glorieux, J. Acoust. Soc. Am. **116**, 2089 (2004).
[11]Y. H. Pao and V. Varatharajulu, J. Acoust. Soc. Am. **59**, 1361 (1976).
[12]R. Briers, O. Leroy, O. Poncelet, and M. Deschamps, J. Acoust. Soc. Am. **106**, 682 (1999).
[13]A. A. Maradudin, X. Huang, and A. P. Mayer, J. Appl. Phys. **70**, 53 (1991).
[14]V. V. Kosachev and A. V. Shchegrov, Ann. Phys. **240**, 225 (1995).

[15]L. Brillouin, *Wave Propagation in Periodic Structures*, (Dover, New York, 1953).
[16]S. E. Sandstrom, J. Acoust. Soc. Am. **79**, 1293 (1986).
[17]A. El-Bahrawy, J. Sound. Vib. **170**, 145 (1994).
[18]T. Kundu, S. Banerjee, and K. V. Jata, J. Acoust. Soc. Am. **120**, 1217 (2006).
[19]D. Leduc, A.-C. Hladky, B. Morvan, J.-L. Izbicki, and P. Pareige, J. Acoust. Soc. Am. **118**, 2234 (2005).
[20]W. Lauriks and L. Kelders, Ultrasonics **36**, 865 (1998).
[21]C. Potel and M. Bruneau, J. Sound Vib. **313**, 738 (2008).
[22]T. Valier-Brasier, C. Potel, and M. Bruneau, J. Appl. Phys. **106**, 034913 (2009).
[23]T. Valier-Brasier, C. Potel, and M. Bruneau, Appl. Phys. Lett. **93**, 164101 (2008).
[24]T. Valier-Brasier, C. Potel, and M. Bruneau, J. Appl. Phys. **108**, 074910 (2010).
[25]M. Bruneau and T. Scelo (translator and contributor), *Fundamentals of Acoustics* (ISTE, UK, 2006).
[26]P. M. Morse and H. Feshbach, *Methods of Theoretical Physics, Part II* (McGraw-Hill, New York, 1953).
[27]D. Royer and E. Dieulesaint, *Elastic Waves in Solids, I* (Springer, New York,2000).
[28]Ph. Gatignol, C. Potel, and N. Bedrici, Appl. Phys. Lett. **96**, 044103 (2010).
[29]B. Morvan, A.-C. Hladky-Hennion, D. Leduc, and J. L. Izbicki, J. Appl. Phys. **101**, 114906 (2007).
[30]C. Potel, D. Leduc, B. Morvan, C. Depollier, A.-Ch. Hladky-Hennion, J.-L. Izbicki, P. Pareige, and M. Bruneau, J. Appl. Phys. **104**, 074908 (2008).